# Volumetric Ultrasound Imaging Using 2-D CMUT Arrays

Ömer Oralkan, *Student Member, IEEE*, A. Sanlı Ergun, *Associate Member, IEEE*, Ching-Hsiang Cheng, Jeremy A. Johnson, *Student Member, IEEE*, Mustafa Karaman, *Member, IEEE*, Thomas H. Lee, *Member, IEEE*, and Butrus T. Khuri-Yakub, *Fellow, IEEE*

***Abstract*—Recently, capacitive micromachined ultrasonic transducers (CMUTs) have emerged as a candidate to overcome the difficulties in the realization of 2-D arrays for real-time 3-D imaging. In this paper, we present the first volumetric images obtained using a 2-D CMUT array. We have fabricated a 128 × 128-element 2-D CMUT array with through-wafer via interconnects and a 420-$\mu$m element pitch. As an experimental prototype, a 32 × 64-element portion of the 128 × 128-element array was diced and flip-chip bonded onto a glass fanout chip. This chip provides individual leads from a central 16 × 16-element portion of the array to surrounding bondpads. An 8 × 16-element portion of the array was used in the experiments along with a 128-channel data acquisition system. For imaging phantoms, we used a 2.37-mm diameter steel sphere located 10 mm from the array center and two 12-mm-thick Plexiglas plates located 20 mm and 60 mm from the array. A 4×4 group of elements in the middle of the 8 × 16-element array was used in transmit, and the remaining elements were used to receive the echo signals. The echo signal obtained from the spherical target presented a frequency spectrum centered at 4.37 MHz with a 100% fractional bandwidth, whereas the frequency spectrum for the echo signal from the parallel plate phantom was centered at 3.44 MHz with a 91% fractional bandwidth. The images were reconstructed by using RF beamforming and synthetic phased array approaches and visualized by surface rendering and multiplanar slicing techniques. The image of the spherical target has been used to approximate the point spread function of the system and is compared with theoretical expectations. This study experimentally demonstrates that 2-D CMUT arrays can be fabricated with high yield using silicon IC-fabrication processes, individual electrical connections can be provided using through-wafer vias, and flip-chip bonding can be used to integrate these dense 2-D arrays with electronic circuits for practical 3-D imaging applications.**

Manuscript received December 17, 2002; accepted May 30, 2003. This work was supported by the United States Office of Naval Research and CBYON, Inc.

Ö. Oralkan is with the Edward L. Ginzton Laboratory, Stanford University, Stanford, CA 94305-4088 and the Center for Integrated Systems, Stanford University, Stanford, CA 94305-4070, USA (e-mail: ooralkan@stanford.edu).

A. S. Ergun, C-.H. Cheng, and B. T. Khuri-Yakub are with the Edward L. Ginzton Laboratory, Stanford University, Stanford, CA 94305-4088, USA.

M. Karaman is with the Department of Electronics Engineering, Işık University, 80670 İstanbul, Turkey.

J. A. Johnson is with the Image Guidance Laboratory, Department of Neurosurgery, School of Medicine, Stanford University, Stanford, CA 94305-5327, USA.

T. H. Lee is with the Center for Integrated Systems, Stanford University, Stanford, CA 94305-4070, USA.

## I. Introduction

The acquisition and display of volumetric information using different imaging modalities have long been subjects of extensive research efforts for both medical and underwater applications. Conventionally, 3-D spatial information is either compressed into 2-D images in the form of projection planes from multiple angles or represented as different cross-sectional planes [1]. In medical applications, the inability to view the complete 3-D anatomy might result in misdiagnosis if the imaging angles and cross sections are not chosen properly [2]. In underwater applications, the lack of 3-D imaging capability makes it more difficult to recognize and classify underwater objects [3]. In the medical field, computed tomography (CT) and magnetic resonance imaging (MRI) have been widely used for volume scanning. The data acquisition rates of CT and MRI scanners are not high enough to generate real-time images of nonstationary tissue. Compared with CT and MRI, ultrasound offers real-time interactive visualization using low-cost, portable equipment with no ionizing radiation.

Most of the existing 3-D ultrasound imaging systems make use of conventional 1-D transducer arrays. A series of 2-D images are acquired by physical movement of the array and rendered into a 3-D image. These systems differ only in the method used to determine the position and orientation of the acquired 2-D images. These methods include mechanical scanning and free-hand techniques based on position estimation, image correlation, magnetic, optical, or acoustic sensing [2], [4]. A disadvantage of these systems is the limitation on the data acquisition rate due to the fact that the volume is scanned by physical movement. This type of a system is too slow to allow real-time imaging of dynamic structures, such as a beating heart. Another disadvantage is the poor spatial resolution of the 1-D arrays in the elevation direction. This poor elevational resolution results in blurry 3-D images, degrades the spatial resolution on the resliced images, and limits the accuracy of volume measurements [5]. An alternative data acquisition method for 3-D ultrasound imaging is the use of a 2-D transducer array, which enables features, such as electronic focusing and beam steering, in both azimuthal and elevational directions [6], [7]. The electronic scanning, using a 2-D array, greatly speeds up the data acquisition and provides uniform resolution in both azimuthal and elevational directions (assuming a symmetric 2-D array).

Element size has presented major difficulties, which have limited the feasibility of 3-D ultrasound imaging using 2-D arrays. The spatial sampling criterion specifies that the maximum element width (equivalently, spacing) must be less than half the acoustic wavelength at the operating frequency in order to prevent grating lobes from appearing in the image. This criterion only applies in the direction in which beams are to be steered. Since 1-D arrays steer beams along a single direction, there is no limit on the element length in the other direction. The 2-D arrays focus and steer beams in both azimuthal and elevational directions; thus, the sampling criterion applies to both dimensions of the array. This requirement critically limits the element area. The small size of the elements causes degradation in output acoustic power and receive sensitivity.

There are also severe difficulties in fabricating these densely populated 2-D arrays and providing individual electrical connections to each element. Efforts for fabricating 2-D ultrasonic transducer arrays date back to early 1970s [8]–[10]. Several other research efforts to fabricate 2-D arrays using piezoelectric materials, such as lead zirconate titanate (PZT) [6], [11]–[15] and 1-3 piezoelectric composites [16], have recently been reported. Several interconnection schemes have been proposed for 2-D arrays. These schemes include multilayer flexible circuits [17], [18], pad grid arrays utilizing flexible printed circuits and miniature coaxial cables [19], and flip-chip bonding [16]. In addition to difficulties in fabricating and interconnecting 2-D transducer arrays, there are also challenges in acquiring and processing data from a large number of ultrasound channels. To reduce the system complexity and cost, synthetic aperture [20], sparse array [21], [22], and subaperture processing [23]–[25] techniques have been proposed. Continuous advancement in microelectronics significantly improves the data acquisition and processing capability of systems employing a large number of channels.

In summary, there is a great need for low-cost, portable, real-time volumetric imaging systems. However, due to limitations in the existing transducer array and interconnect technologies, full-scale 3-D imaging systems have not yet been successfully realized. The CMUT technology is a strong candidate to overcome the technical challenges mentioned above [26]. The CMUTs are fabricated using standard silicon IC technology; therefore, it is possible to make large arrays using simple photolithography. Individual electrical connections to transducer elements in these arrays are provided by through-wafer interconnects. The 2-D CMUT arrays having as many as $128 \times 128$ elements have already been successfully fabricated and characterized [27]. In addition to the ease of manufacturing CMUTs, there are major performance advantages compared with piezoelectric transducers, such as improved bandwidth and sensitivity and potential for electronic integration. We have previously reported the fabrication process for 1-D and 2-D CMUT arrays [28]–[30]. We have also characterized these arrays in terms of the performance of a single element in transmit and receive modes [31], [32]. We have recently demonstrated the first full-scale phased-array images using a 128-element linear array based on the CMUT technology [33].

In this paper, we present the first volumetric images obtained using a 2-D CMUT array. The significance of this study is that we experimentally demonstrate that 2-D CMUT arrays can be fabricated with high element yield using silicon IC-fabrication processes, individual electrical connections can be provided using through-wafer vias, and flip-chip bonding can be used to integrate these dense 2-D arrays with electronic circuits for practical 3-D imaging applications. The organization of this paper is as follows. Section II briefly describes the 2-D CMUT arrays used in this study. The experimental methods used are explained in Section III. The results are presented in Section IV.

## II. 2-D CMUT Arrays

The basic principles of operation and the fabrication process of CMUTs have been previously reported [28], [29]. A metalized membrane suspended over a heavily doped silicon substrate forms a single capacitor cell, which is the basic building block of a CMUT. The cross section of a single capacitor cell is schematically depicted in Fig. 1(a). A group of these capacitor cells connected in parallel constitute an element in a 2-D array. Each element in the 2-D array is individually addressable using a through-wafer via interconnect. A 3-D visualization of a single element with a through-wafer via interconnect is shown in Fig. 1(b). The through-wafer vias are formed by the use of deep reactive ion etching from both sides of the wafer. The top view of a via hole is shown in Fig. 1(c). The doped polysilicon in the via provides the electrical connectivity between the back electrode of the array element in the front and the electrical connection pad on the back side of the silicon substrate. A scaning electron microscope (SEM) picture shows the cross section of a finished through-wafer via interconnect in Fig. 1(d). The top electrode is common to all the elements in the array, and the back electrodes are isolated islands of doped polysilicon on the silicon substrate, each electrically accessible from the back side. The common top electrode can be seen as a meshed structure in Fig. 1(e) in which the top view of a portion of a 2-D array is shown. The top view of a single element and a close-up of individual cells are shown in Fig. 1(f) and (g), respectively. A detailed description of the fabrication process for 2-D arrays with through-wafer via interconnects can be found in [27], [30]. The physical dimensions of the 2-D CMUT array used in this work are listed in Table I.

The first generation of 2-D CMUT arrays with through-wafer via interconnects suffered from a large parasitic capacitance ($\sim$2 pF) in parallel with the device capacitance [34]. This parasitic capacitance has been reduced in later generations of through-wafer interconnects to a value of 50 fF by employing reverse-biased pn junction diodes [27], [30]. The reduction of parasitics is critical to achieve good receive sensitivity and preserve wide bandwidth, especially for 2-D array elements in which the individual

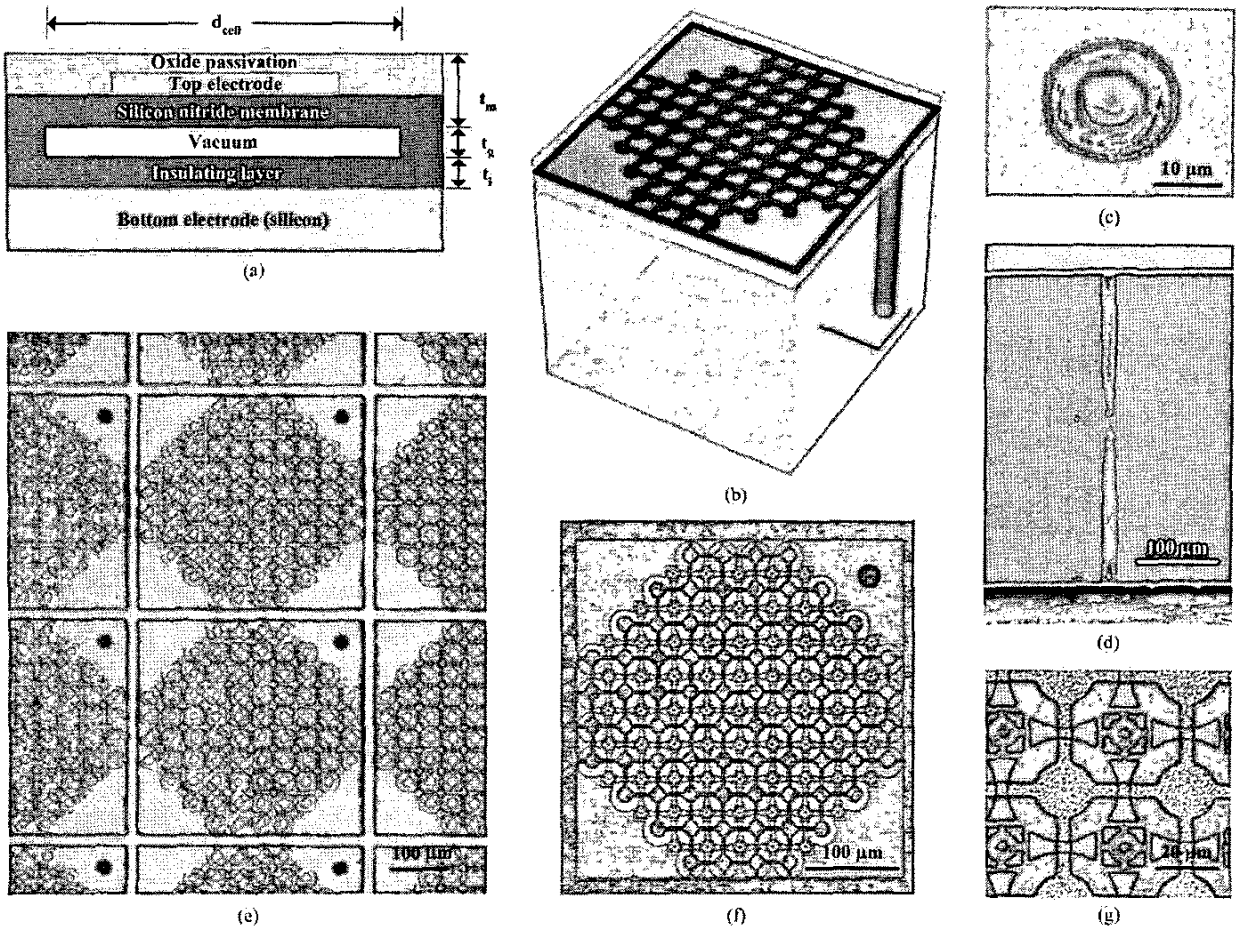


Fig. 1. 2-D CMUT array. (a) Schematic cross section of a CMUT cell. (b) 3-D model of a CMUT cell with a through-wafer via interconnect. (c) Top view of a through-wafer via. (d) SEM cross section of a through-wafer via. (e) Top view of multiple 2-D CMUT elements forming an array. (f) Top view of a single 2-D CMUT array element. (g) Top view of individual CMUT cells constituting 2-D array elements.

TABLE I
PHYSICAL PARAMETERS OF THE 2-D CMUT ARRAY.

| | |
|---|---|
| Element pitch ($d$), $\mu$m | 420 |
| Size of an element, $\mu$m × $\mu$m | 400 × 400 |
| Number of cells per element | 76 |
| Cell diameter ($d_{cell}$), $\mu$m | 36 |
| Membrane thickness ($t_m$), $\mu$m | 0.65 |
| Gap thickness ($t_g$), $\mu$m | 0.1 |
| Insulating layer thickness ($t_i$), $\mu$m | 0.2 |
| Silicon substrate thickness, $\mu$m | 400 |

device capacitance is very small. To integrate 2-D transducer arrays with associated transmit/receive electronics, as briefly discussed in Section I, several different interconnection schemes have been proposed in the literature. Monolithic integration of CMUTs with electronic circuits has also been proposed [35]–[38]. Monolithic integration of microelectromechanical systems (MEMS) with electronic circuits usually results in a compromise of the performance of one or both components. It has been demonstrated that a modified CMOS or BiCMOS process could be used to fabricate ultrasonic transducers on the same silicon substrate with electronic circuits [35], [36]. Although this method provides a cost-effective means of integration, it is not suitable for 2-D arrays because the usable active area is compromised either by the electronics, if the element area is shared with the electronics, or by the interconnect lines, if the electronics is placed on the periphery of the array and connected to the array elements through routing lines. In this approach, the number of available design parameters is also reduced due to the use of a standard process. An alternate method uses postprocessing to fabricate CMUT elements over the electronics chip, which is built using a standard CMOS process [37], [38]. The wafer with the electronics goes through passivation and CMP processes before the CMUT fabrication process. This integration method, probably being slightly costlier than the former, is suitable for 2-D array integration because of its better area utilization. Because the preprocessed electronics limits the temperature of the postprocesses, a low temperature process must be used to fabricate CMUTs over the electronics. Although the low temperature CMUT

process, which uses plasma enhanced chemical vapor deposition, has been tailored to achieve good control over the stress in the membrane and reasonable uniformity, high temperature CMUT process, which uses low-pressure chemical vapor deposition, still result in better on-wafer and wafer-to-wafer uniformity and higher yield. The integration method we describe in this paper proposes to fabricate the electronics and the transducers on separate wafers and to integrate them with flip-chip bonding. In this way, high temperature processes can be used to fabricate high-density and high-performance CMUT arrays with high yield and uniformity. The integration of the CMUT array with the electronics comes at the expense of additional steps to the CMUT process, which are the fabrication of the through-wafer interconnects to bring the electrical connections to the back side of the silicon wafer and flip-chip bonding. Both of these processes are CMOS compatible. Because the electronics and the transducer arrays are fabricated on separate wafers, the overall yield of the manufacturing process is enhanced, and the turn-around time is reduced. The cost reduction associated with the higher yield and faster turn-around time compensates (probably surpasses) the increase in the cost due to the increase in the number of steps. The integration of array elements with electronics on the probe does not only improve the performance but also reduces the number of external leads to a manageable level. A similar approach was also taken previously in which custom designed integrated circuits were wire-bonded at the back side of a 2-D ultrasonic transducer array [39].

## III. Experimental Work

The experimental system used in this study was originally designed for data acquisition from a 128-element, 1-D linear CMUT array. This PC-based data acquisition system consists of a PC and electronic circuits implemented on printed circuit boards (PCBs) using off-the-shelf electronic components.

A custom fanout assembly was built such that the 2-D CMUT array could be tested without modification to the existing experimental apparatus. A 128 × 128-element 2-D CMUT array was diced into 32 × 64-element arrays so that it could be flip-chip bonded onto another chip. We mounted one of these 32 × 64-element CMUT arrays employing through-wafer vias [Fig. 2(a)] to a glass substrate that provides individual leads from the elements of a 16 × 16-element subsection to pads surrounding the array [Fig. 2(c)]. This fanout chip was fabricated using a standard liftoff process following a chromium-gold deposition on a glass substrate. The 3-D multichip assembly is schematically depicted in Fig. 2(b). The CMUT array-glass substrate assembly was mounted and wire-bonded onto a PCB as shown in Fig. 2(d). Individual bond wires for active elements and ground connections can be seen in the magnified view of the center portion of the PCB [Fig. 2(e)]. Half of the 16 × 16-element array was used in this experiment due to the channel count limitation of the existing 128-channel data acquisition system. Although we would eventually like to bond the 2-D CMUT array onto a silicon integrated circuit, for initial imaging experiments, we used a glass fanout chip that allows us to use the 2-D arrays with the existing experimental data acquisition system.

The experimental setup is schematically shown in Fig. 3 with illustrations of the imaging phantoms. The PCB carrying the 2-D CMUT array was connected to a PCB that provided the dc bias to the transducer elements and ac coupled the transmit and receive signals to and from the array, respectively. A second stage of electronic circuits provided transmit and receive channel selection and amplification of the incoming echo signals. Further details of the experimental data acquisition system can be found in [33]. Due to the use of board-level discrete electronics, the parasitic capacitance was more than 20 pF, whereas the device capacitance was only 1 pF. This excessive parasitic capacitance significantly degrades the SNR of the acquired echo signals. To improve the SNR of the acquired A-scans, we have synthesized a powerful virtual transmit element by connecting 4 × 4 elements (at the center of the 8 × 16 array) in parallel without any phasing as shown in Fig. 4. The remaining elements in the array were used for receive. The transmitting elements were not used for receive because the SNR of the received echo signals was low when the same channel was active both in transmit and receive simultaneously. This low SNR is due to the use of off-the-shelf electronic switches and board-level electronics. A high-voltage dc supply was used to provide the 20-V bias voltage for the 2-D CMUT array, so that the array elements are biased close to collapse for maximum sensitivity[1]. The polarity of the dc bias voltage was chosen so that the pn junctions formed around the through-wafer vias would be reverse-biased. A function generator was used for pulsed excitation of the transducer elements. A 15-V, 100-ns rectangular pulse was applied to transducer elements to generate the ultrasound signals. The echo signals were amplified by a fixed gain of 60 dB. The amplified signals were sampled at a rate of 100 MHz and digitized with a resolution of 8 bits. In this experiment, 100 successive A-scan acquisitions were averaged to further improve

[1]Although the dimensions of the devices used in this study are almost identical to the ones reported in [31], there is a significant difference in the fabrication process. In earlier CMUTs, the etch channels and the active areas were not defined separately, and the final membrane thickness was adjusted by an etch-back process. As a result, the posts were thicker than the membrane. To achieve a better control on gap and membrane thicknesses and to improve the reliability of the devices, we separated the etch channel and the active are definitions, so that the etch channels can be made thin, consequently easy to seal [40]. In this process, minimum amount of nitride is deposited inside the membrane and on the posts. Consequently, the posts are thinner compared with earlier devices. The residual tensile stress in the membrane and the atmospheric pressure cause an inward deflection in the membrane [41]. When the posts are thinner, they bend inward more easily, resulting more deflection in the membrane and a lower collapse voltage. In the experiments described in this paper, to increase the efficiency of the device, we operated the transducers close to the collapse voltage, which was lower than that of earlier devices.

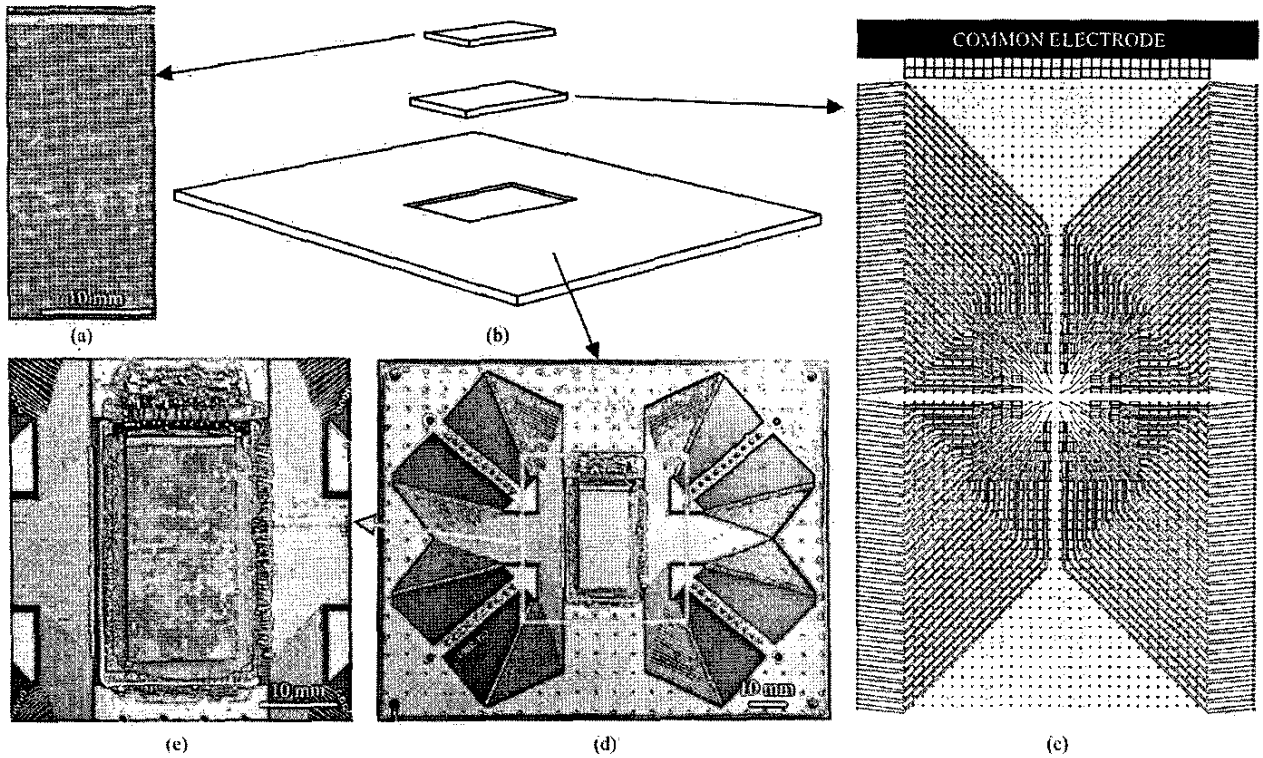


Fig. 2. 2-D array assembly. (a) $32 \times 64$ 2-D CMUT array diced from a $128 \times 128$-element array. (b) Schematic representation of 3-D multichip assembly. (c) Top view of the glass carrier chip layout to fan out a $16 \times 16$ portion of the 2-D CMUT array. (d) The printed circuit board (PCB) carrying the flip-chip-bonded 2-D array-glass substrate assembly. (e) Magnified view of the center portion of the PCB showing the wire bonds from glass substrate to the PCB.

the SNR of A-scans. The averaged A-scans were stored with a 12-bit sample resolution for offline digital processing.

We used two different custom-built imaging phantoms in this study. The first phantom consisted of two Plexiglas plates parallel to the transducer array, each 12 mm thick and 30 mm apart from each other. The plates were attached to each other using a thin plastic bar at the center. The second phantom was a spherical target made of steel with a diameter of 2.37 mm. The steel sphere was attached to the tip of an acrylic fiber supported by a Plexiglas base. Both phantoms and the CMUT array were immersed in vegetable oil during the experiments. Vegetable oil roughly mimics the attenuation of soft tissue and provides a natural isolation between the unisolated bond wires. We have previously measured and reported the attenuation characteristics of vegetable oil [33].

## IV. Experimental Results

2-D CMUT arrays have already been experimentally characterized in transmit and receive modes, and the results have been compared with theoretical expectations [31]. The results that are presented here complement the results obtained earlier. However, experiments performed in this study focus on the demonstration of volumetric imaging using 2-D CMUT arrays rather than their characterization in terms of their receive and transmit performance.

### *A. Analysis of A-scan Data*

We have measured the one-way radiation pattern of a single 2-D array element, compared the measurements to theory, and demonstrated the CMUT array element exhibits a piston-like behavior [42]. The 6-dB acceptance angle was measured as $\pm 50$ in agreement with the theoretical prediction when the transducer was operated at 3 MHz. The theoretical 6-dB acceptance angle for the $4 \times 4$ subgroup of transducers is $\pm 14$ and $\pm 8$ degrees for 3- and 5-MHz operation, respectively. As we have discussed in the previous section, a $4 \times 4$ group of transducer elements was fired simultaneously without any phasing. This approach increases the total acoustic power transmitted, improving the SNR of the received echo signals. However, the use of multiple transducer elements in parallel with no phasing is equivalent to using a single large transducer element in transmit and results in a narrow transmit beamwidth. Consequently, a very small area was insonified by the narrow beam formed by the unphased $4 \times 4$ group of transmitting transducer elements. The positions of the target and the receiving transducer element significantly affect the received echo signal due to the narrow transmit beam. Therefore, the A-scans presented in this section do not correspond to an accurate pulse-echo impulse response of

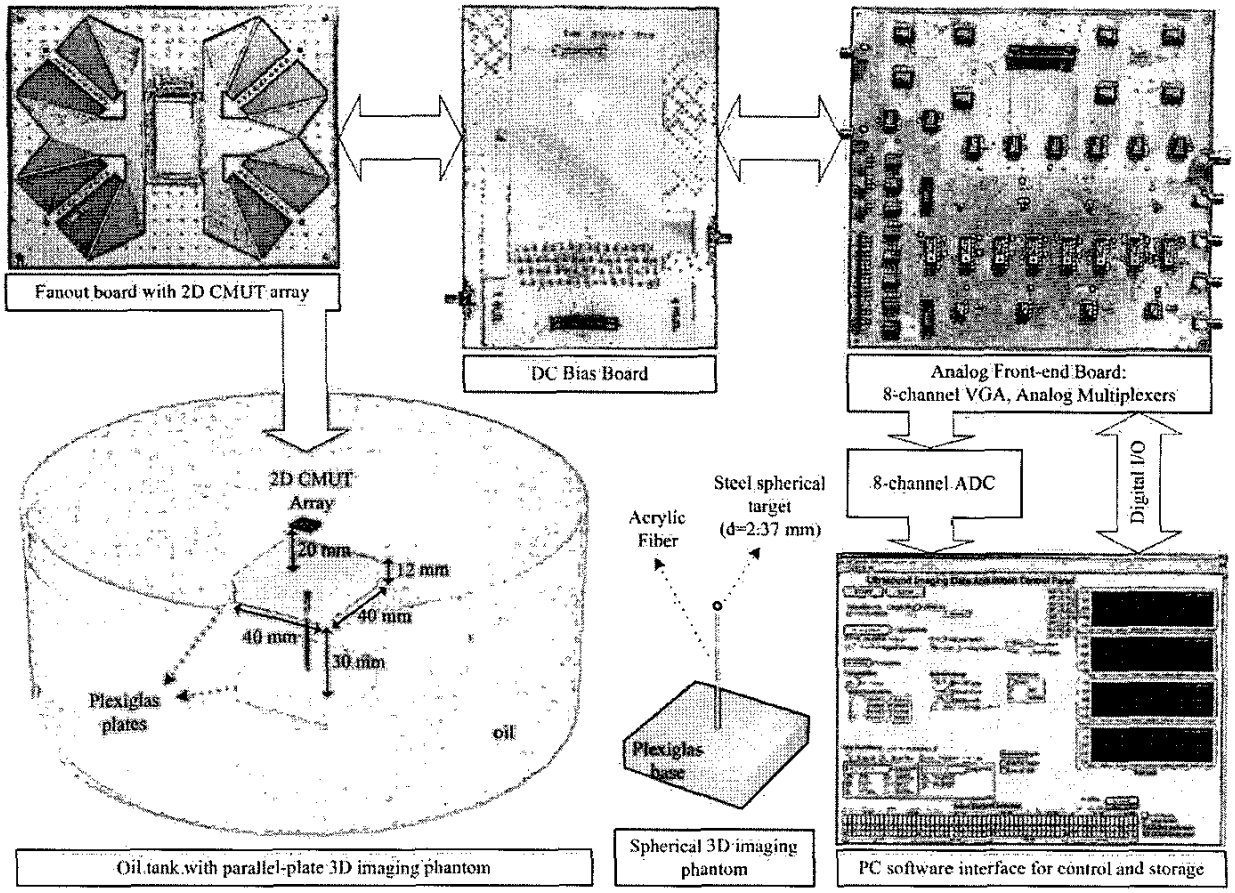


Fig. 3. Experimental setup with 3-D imaging phantoms.

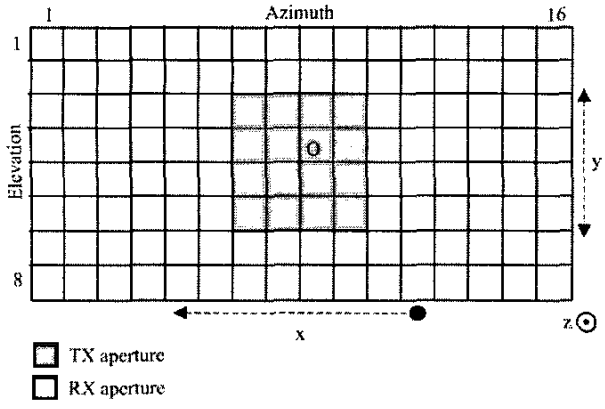


Fig. 4. Schematic view of the 8 × 16 2-D array showing the transmit and receive apertures and the coordinate axes.

a 2-D CMUT array element. Representative impulse response measurements for 2-D CMUT array elements can be found in [42].

A sample echo signal received by a single element and reflected from the top surface of the parallel-plate phantom is shown in Fig. 5(a). A 1- to 5-MHz digital bandpass filter was applied in addition to a 5-MHz lowpass filter used during the data acquisition. These filters were used to eliminate out-of-band noise in the received A-scans. The corresponding frequency spectrum is shown in Fig. 5(b). This echo signal presented a 91% fractional bandwidth centered at 3.44 MHz and includes the effects of frequency dependent attenuation and diffraction in the propagating medium. The total round-trip distance was around 50 mm for this pulse.

A sample echo signal received from the spherical target is shown in Fig. 6(a). Because the target was only 10 mm from the array, the frequency spectrum was less severely affected by the attenuation compared with the spectrum shown in Fig. 5(b). A 10-MHz lowpass filter was used during data acquisition in this experiment. The received A-scan was further filtered using a 1- to 8-MHz digital bandpass filter to eliminate out-of-band noise. The resulting pulse-echo frequency spectrum was centered at 4.37 MHz with a fractional bandwidth of 100% as shown in Fig. 6(b).

### *B. Image Reconstruction and Visualization*

We digitally processed the raw RF A-scan data to reconstruct the phased array volumetric images. The im-

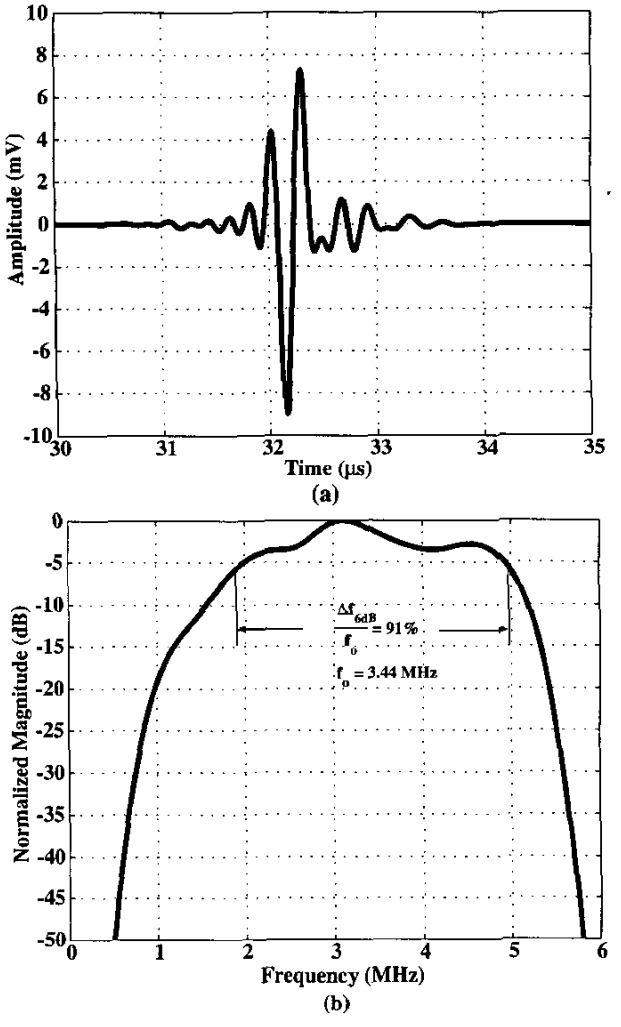


Fig. 5. (a) Measured echo signal from the top surface of the plate phantom. (b) Corresponding frequency spectrum.

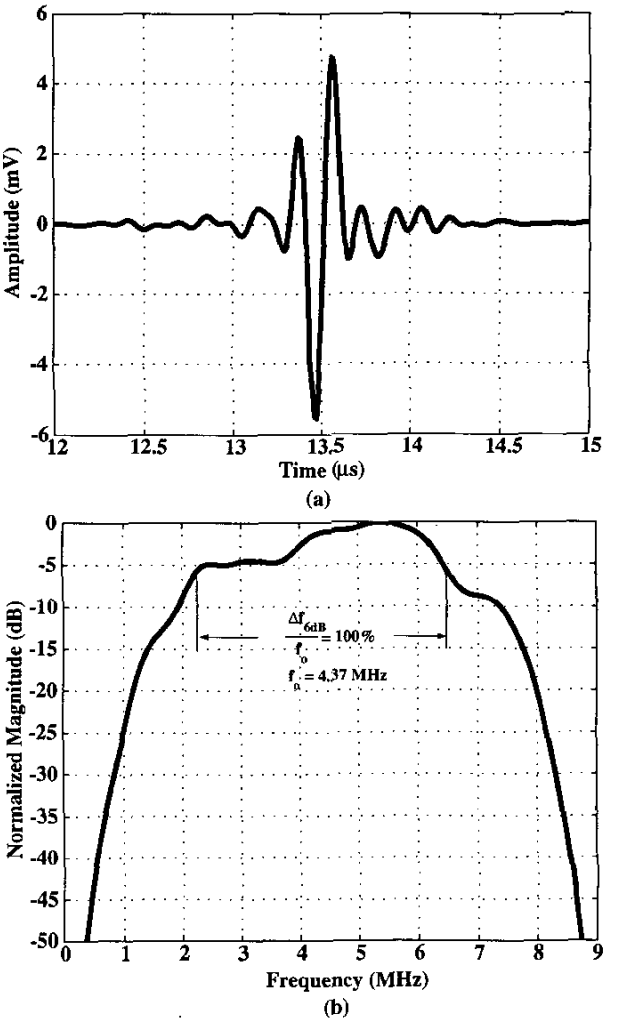


Fig. 6. (a) Measured echo signal from the spherical phantom. (b) Corresponding frequency spectrum.

ages were reconstructed by employing RF beamforming and synthetic phased array approaches [20], [33], [43]. The basic principles of beam steering with 2-D arrays have been previously explained [6], [44], in which a conical or pyramidal volume has been scanned. We chose to scan a cubic volume in which the individual volume elements (voxels) were arranged in a cartesian grid in three dimensions. We have also used the pyramidal scan approach to reconstruct the volumetric image of the spherical phantom. Due to the use of a fixed transmit aperture, only dynamic receive focusing was employed. The coordinate system used is shown in Fig. 7. The origin of the coordinate system is the center of the $8 \times 16$-element array for both the cartesian and the pyramidal scan. $\theta$ is the steering angle in the azimuth direction. The steering angle in the elevation direction is $\phi$, and $\rho$ is the distance in the radial direction. The conventional right-hand cartesian coordinate axes are $x$, $y$,

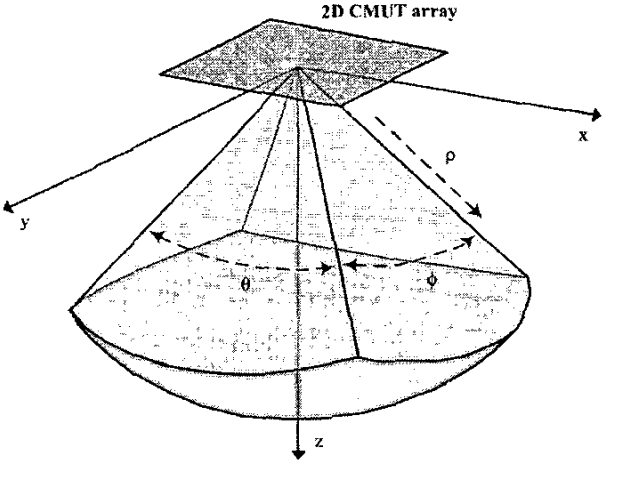


Fig. 7. 3-D coordinate system used for image reconstruction.

and $z$. Image reconstruction in cartesian coordinates can be expressed as

$$U[p,q,r] = \sum_{m=1}^{M}\sum_{n=1}^{N} s_{mn}[k], \tag{1}$$

where

$$k = round\{f_s(t_f - t_0)\}, \tag{2}$$

$$t_f = \frac{1}{c}(\rho[p,q,r,0,0] + \rho[p,q,r,m,n]). \tag{3}$$

Here, $U[p,q,r]$ is the value of the image voxel in cartesian coordinates represented by sample indices $(p,q,r)$. The indices $p$, $q$, and $r$ correspond to the coordinate axes $x$, $y$, and $z$, respectively. $M$ and $N$ are the size of the 2-D array in azimuth and elevation directions, respectively. The digitized RF A-scans are represented by $s_{mn}$, where the subscripts $m$ and $n$ correspond to the row and column addresses of the receiving element. The total time of flight, $t_f$, is the sum of the times of flights from the transmitter to a voxel $(\rho[p,q,r,0,0]/c)$ and from that voxel back to the receiver $(\rho[p,q,r,m,n]/c)$. $t_0$ is the offset time, $f_s$ is the sampling frequency of A-scans. The rounding operation in (2) is performed to pick the closest sample to the calculated exact time point.

The beamforming for the pyramidal scan is similar to that of the cartesian scan, only with different geometrical considerations. The relation between the 3-D coordinate systems for cubic and pyramidal scans is described by the following set of equations:

$$\rho_v = \sqrt{x_v^2 + y_v^2 + z_v^2}, \tag{4}$$

$$x_v = z_v \tan\theta_v, \tag{5}$$

$$y_v = z_v \tan\phi_v, \tag{6}$$

where $\theta_v$ and $\phi_v$ are the steering angles in azimuth and elevation directions, respectively, and $\rho_v$ is the distance between a voxel $V(\theta_v, \phi_v, \rho_v)$ and the origin. The same voxel is represented as $V(x_v, y_v, z_v)$ in cartesian coordinates.

The visualization and analysis of 3-D data is an area of research by itself [45]. The visualization of 3-D ultrasound data is also the focus of significant research efforts [46]. Multiplanar slicing, surface fitting, and volume rendering are three basic techniques for volume visualization. This paper focuses on the acquisition of 3-D ultrasound data rather than its visualization, and hence the simplest methods have been employed to visualize the resulting volumetric images. In this paper, we present surface-rendered 3-D images, in which planar surface primitives, such as patches, were fit to constant-value contour surfaces in the volumetric data set. We also present slices of the volumetric data on a grayscale display. The volumetric data sets were logarithmically compressed prior to visualization.

### C. Reconstructed Images

The reconstructed experimental images of the parallel-plate phantom are shown in Fig. 8. Fig. 8(a) and (c) show the center cross sections in the elevation and azimuth directions, respectively. The display dynamic range of these grayscale images is 40 dB. A surface-rendered visualization of the 16-cm$^3$ volume is shown in Fig. 8(b). The surface rendering was performed using the standard isosurface function in MATLAB (Mathworks Inc., Natick, MA) with an isovalue of 10 dB. The respective positions of the parallel plate phantom and the 2-D array are superimposed on the reconstructed image. The four interfaces corresponding to two faces of two Plexiglas plates are clearly identified in the reconstructed images. The shadowing artifact near the interfaces can be attributed to the crosstalk among the array elements or the reverberation in the target or the backing PCB. Further investigation is needed to pinpoint the origin of these artifacts. As explained earlier, due to the use of a $4 \times 4$ group of unphased transducers, a narrow transmit beam is formed and consequently only a small portion of the phantom is insonified. In addition, since the surface of the plate acts as a strong specular reflecting surface, the reflected wavefronts directed parallel to array normal can be detected by the array, the other reflections fall out of the small aperture. Therefore the resulting image is close to a point spread function (PSF) (one-way diffraction pattern of 2-D rectangular aperture). Note that the reflecting target is effectively a small portion of the plate surface around the array normal. The curved extensions of the image, as expected, correspond to sidelobes of the beam pattern. The surfaces of the plates can be viewed as planar structures on a B-scan image reconstructed using a sufficiently larger aperture. A top view of the surface-rendered 3-D image is shown in Fig. 9. The side-lobe patterns are clearly identified in this top view. As a result of the asymmetric shape of the $8 \times 16$-element 2-D array, the sinc-like side-lobe patterns are not symmetric in azimuth and elevation directions. The mainlobe is narrower and the side-lobe pattern is denser in the azimuth direction corresponding to the wider aperture. Note that since the transmit beam is narrow and fixed, it only insonifies a small portion in the middle of the plates.

The spherical target images better characterize the 3-D PSF of the system. The spherical target we used in our experiments was 2.37 mm in diameter, which is several wavelengths at 4.5 MHz. Since this spherical target does not act as a point reflector, the resulting images are only an approximation to the PSF of the system. A surface-rendered visualization of the reconstructed 3-D image is shown in Fig. 10. The mainlobe and sidelobe levels are difficult to identify in the surface-rendered visualization. However, the grating lobes in both azimuth and elevation directions are clearly visible. Center cross sections in the elevation and azimuth directions of the resulting image are shown with a 20-dB display dynamic range in Figs. 11(a) and (c). In these cross-sectional images, the top side of the steel sphere is clearly identified as a strong reflector. However, it is still difficult to perform a quantitative analysis of sidelobe and grating lobe levels on these images. The same cross-sectional images are presented in Figs. 11(b) and (d) with a 40-dB display dynamic range. In these images the

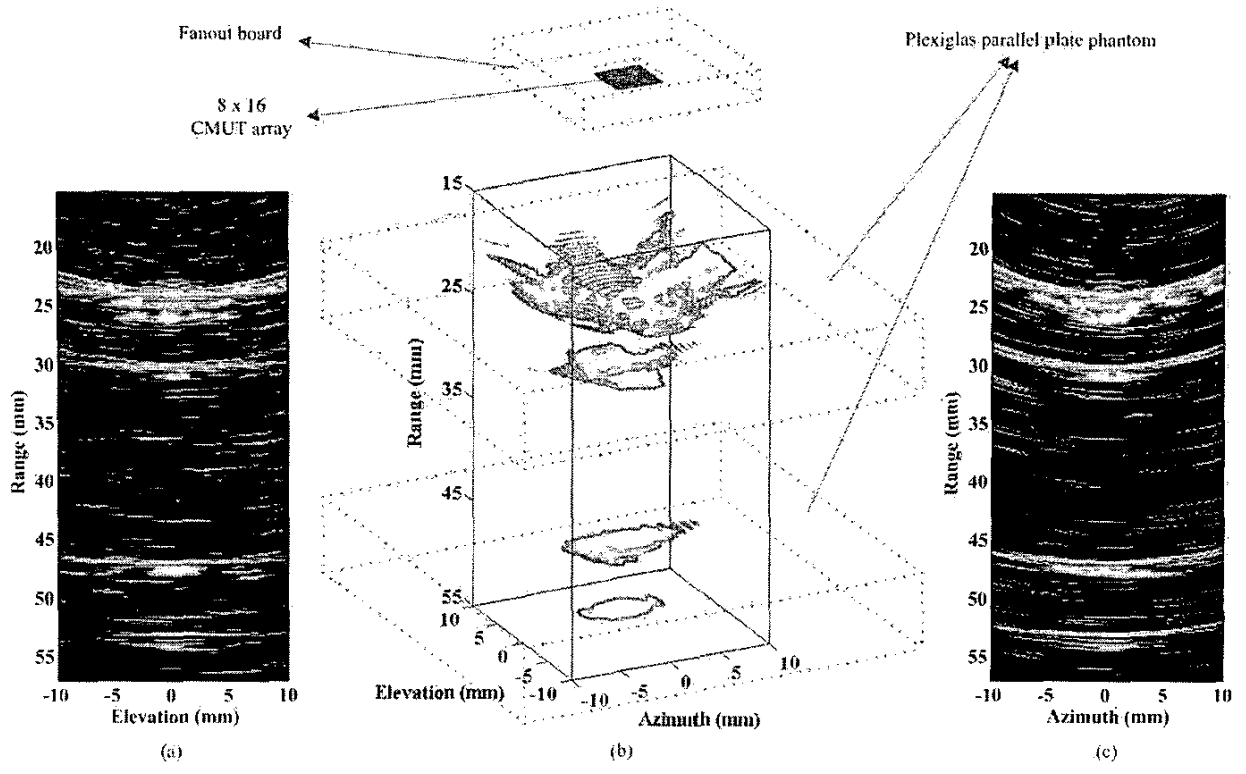


Fig. 8. Reconstructed 3-D image of the parallel plate phantom. (a) Elevational grayscale cross-sectional image with a display dynamic range of 40 dB. (b) Surface-rendered 3-D image superimposed on the parallel plate phantom model. (c) Azimuthal grayscale cross-section image with a display dynamic range of 40 dB.

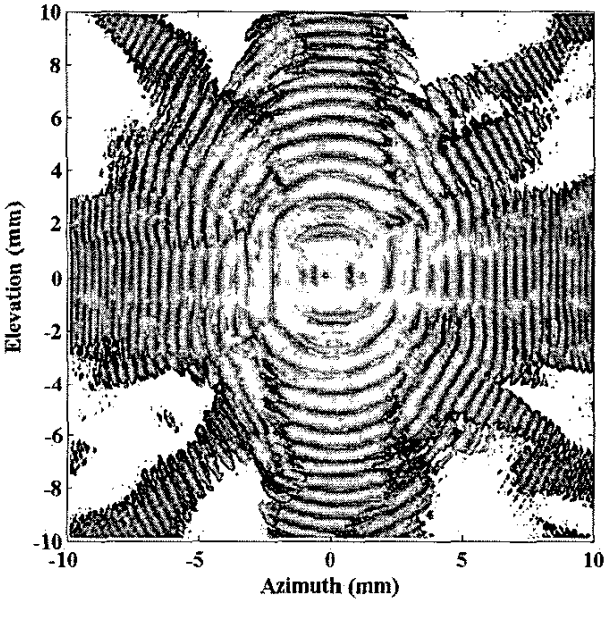


Fig. 9. Top view of the reconstructed 3-D image of the parallel plate phantom.

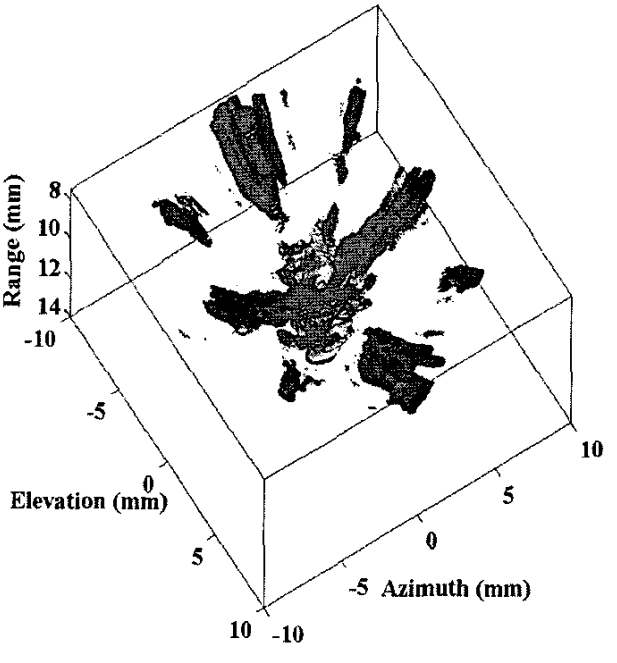


Fig. 10. Surface-rendered 3-D image of the spherical phantom.

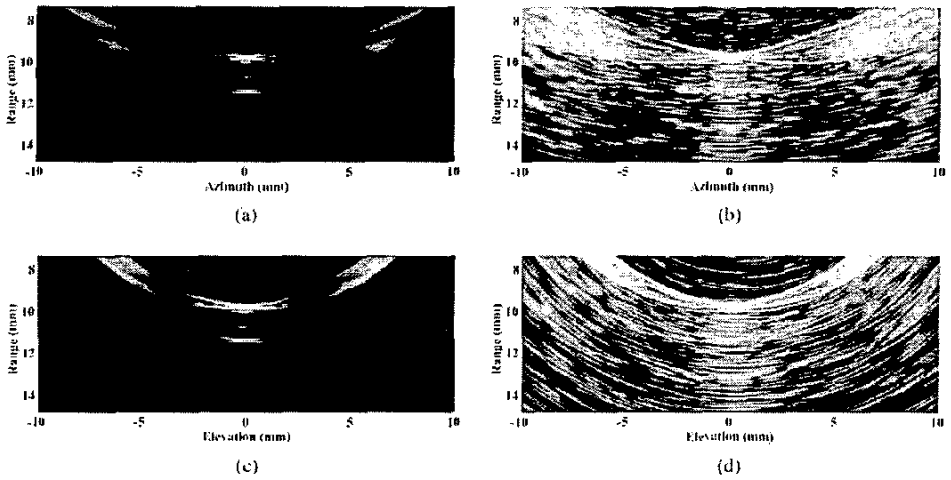


Fig. 11. Cross-sectional images of the spherical phantom. (a) Azimuthal grayscale cross-sectional image with a display dynamic range of 20 dB. (b) Azimuthal grayscale cross-sectional image with a display dynamic range of 40 dB. (c) Elevational grayscale cross-sectional image with a display dynamic range of 20 dB. (d) Elevational grayscale cross-sectional image with a display dynamic range of 40 dB.

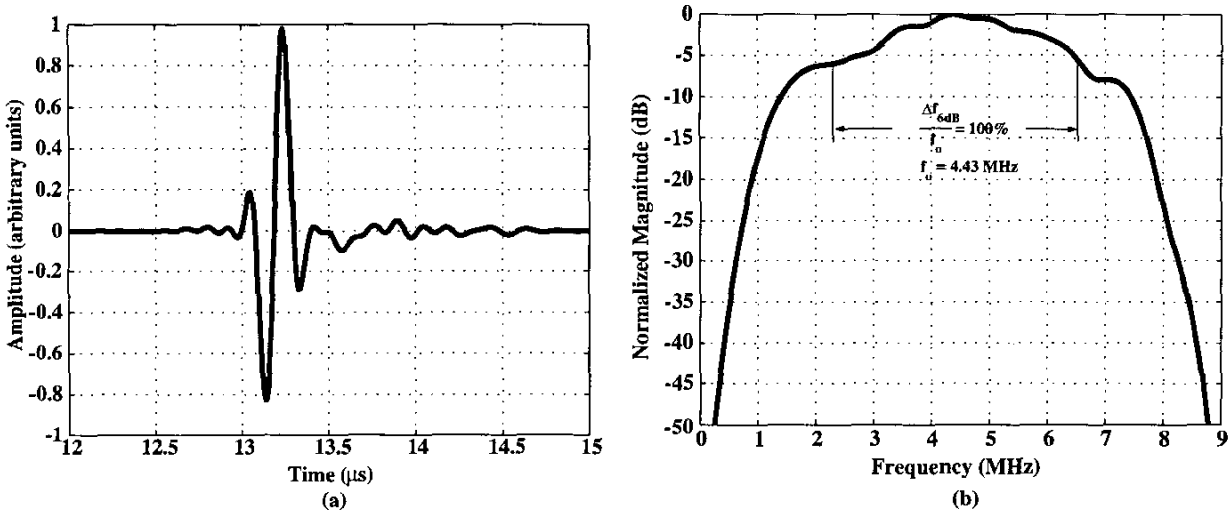


Fig. 12. (a) Simulated echo signal from the spherical phantom. (b) Corresponding frequency spectrum.

artifacts due to the reverberations in the steel sphere and also the electronic noise floor are observable.

A quantitative analysis can better be performed on the constant-range images. In order to conduct this analysis, we reconstructed the images of the spherical phantom using the pyramidal scan approach. We have also reconstructed simulated images to compare the experimental results with theoretical expectations. To have a fair comparison between the experimental and the simulated results, the size of the spherical target should be taken into account. We have modeled the target as a hemispherical mesh of specular reflectors located a quarter wavelength apart from each other. A gaussian-modulated echo signal was assumed from each specular reflector. To obtain a single RF A-scan, the individual echo signals from all specular reflectors were summed together after applying appropriate delays to each echo. The angular response of the transducer elements were also taken into account by applying appropriate weights prior to summation. A simulated A-scan according to this model is shown in Fig. 12(a) along with the corresponding frequency response in Fig. 12(b). This simulation accounted for the angular response of an ideal single transducer element. The set of simulated RF A-scan data was used to reconstruct a 3-D image using the same procedure used for the experimental images. A constant-range cross-sectional image, which intersects the brightest voxel, is shown in Fig. 13(a) for the experimental data. The corresponding simulation result for the hemispherical reflector model is shown in Fig. 13(b). No additive noise was present in the simulation. Good agreement

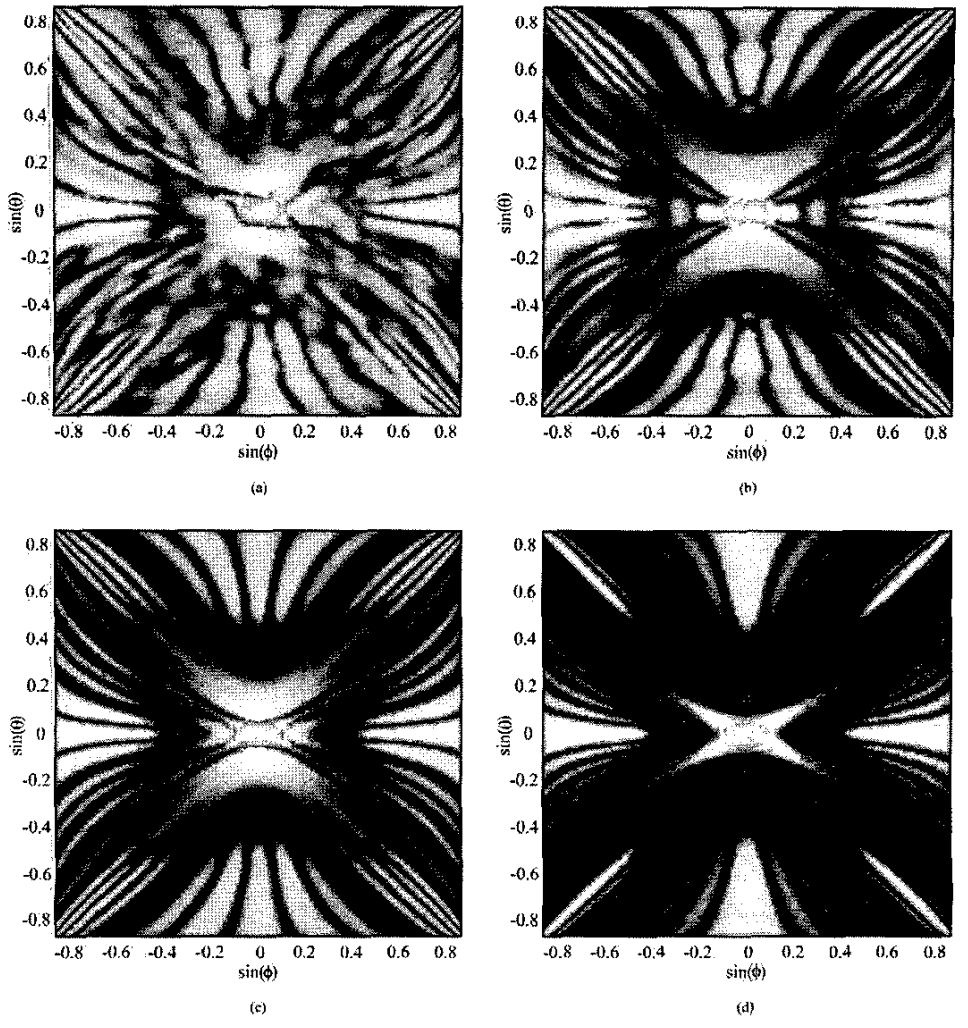


Fig. 13. Grayscale images of the spherical target at a constant range with a display dynamic range of 40 dB. (a) Experiment. (b) Hemispherical reflector model (experimental equivalent). (c) Point reflector model. (d) Point reflector model when full 8 × 16 aperture used for receive.

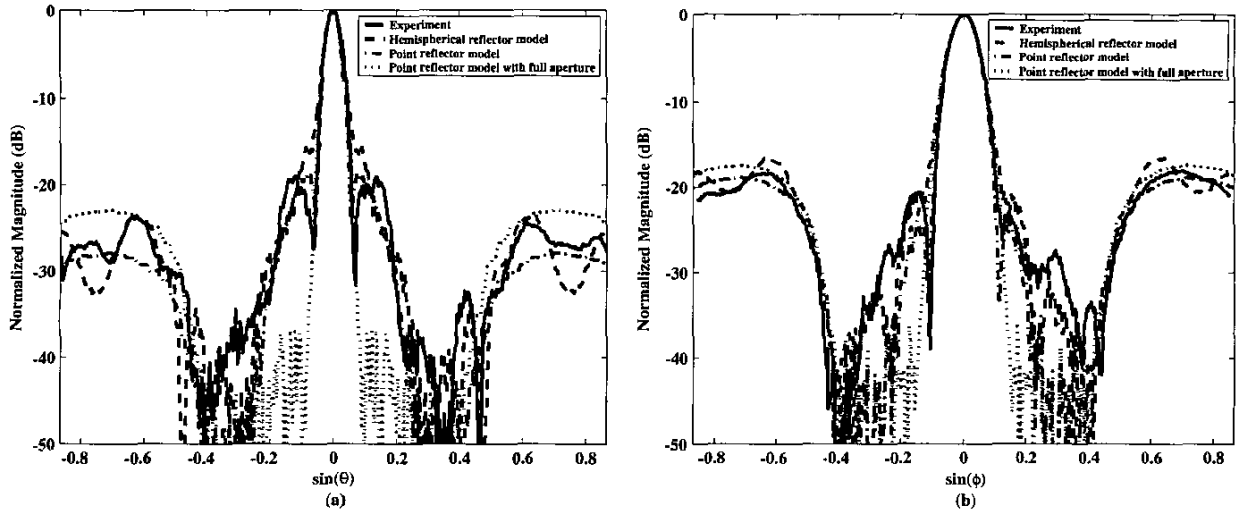


Fig. 14. (a) Azimuthal cross section of the constant range images. (b) Elevational cross section of the constant range image.

is observed between the simulation and the experimental result for all mainlobe, sidelobe, and grating lobe patterns. The 2-D array used in this study was designed with an interelement spacing of 420 $\mu$m for a system with dual-mode operation capability at 750 kHz and 3 MHz. The grating lobes were expected since the frequency of operation was around 4.5 MHz, which translates into an inter-element spacing of approximately 1.3 $\lambda$ for the particular array.

We have also performed a simulation for an ideal point target. The result of this simulation is shown in Fig. 13(c). It can be seen that the simulation result with the ideal point reflector is close to the one with the hemispherical reflector model, suggesting that the obtained experimental result is a good approximation to the PSF of the system. In all of the above simulations and the experimental image reconstruction, we used the A-scans received by the elements outside the central $4 \times 4$ portion of the array. In the experiment, since the $4 \times 4$ group of elements in the middle of the array were used to transmit, we did not use them for receive. Using this type of a hallow aperture actually raises the sidelobe level significantly. We have performed another simulation with the ideal point reflector model in which the complete $8 \times 16$ aperture was used to receive. The resulting constant-range image is shown in Fig. 13(d). The center-line cross sections of the constant-range images are shown in Fig. 14. A good agreement is observed between the experimental results and the simulation results based on the hemispherical reflector model, both in the azimuth and the elevation directions.

## V. Conclusion

In this paper, we presented the first volumetric imaging results using a 2-D CMUT array. In spite of the use of a nonideal experimental setup and a small aperture due to the channel count limitation of the existing data acquisition system, the experimental results provide a proof of concept for 3-D imaging using 2-D CMUT arrays; hence, these results are quite encouraging. This study also experimentally demonstrated that 2-D CMUT arrays can be fabricated with high yield using silicon micromachining, individual electrical connections can be provided using through-wafer vias, and flip-chip bonding can be used to integrate these dense 2-D arrays with electronic circuits for practical imaging applications.

Due to limitations in the existing transducer array and interconnect technologies, more than 20 yr of research in real-time 3-D ultrasound imaging have not yet translated into successful practical results. The CMUT technology makes use of advanced IC-fabrication processes and enables the easy manufacture of large 2-D transducer arrays with individual electrical connections. CMUT is an ideal candidate to replace or complement the existing piezoelectric transducers in many applications. Above all else, we believe that CMUTs will have their greatest impact on the realization of real-time 3-D ultrasound imaging systems.

## Acknowledgments

The authors thank Lockheed-Martin Corporation for flip-chip bonding the array, Aykutlu Dâna, Kambiz Kaviani, and Göksen Yaralıoğlu for useful discussions about instrumentation, Tim Brand for dicing the arrays, Pauline Prather for wire bonding, Larry Randall for his help with machining, and Murat Özsüt and Mehmet Yüksekkaya for their help in data analysis and PCB design.

## References

[1] J. L. Coatrieux, C. Toumoulin, C. Hamon, and L. Luo, "Future trends in 3D medical imaging," *IEEE Eng. Med. Biol. Mag.*, vol. 9, pp. 33–39, Dec. 1990.

[2] A. Fenster, D. B. Downey, and H. N. Cardinal, "Three-dimensional ultrasound imaging," *Phys. Med. Biol.*, vol. 46, pp. R67–R69, May 2001.

[3] V. Murino and A. Trucco, "Three-dimensional image generation and processing in underwater acoustic vision," *Proc. IEEE*, vol. 46, pp. 1903–1946, Dec. 2000.

[4] J. A. Hossack, T. S. Sumanaweera, S. Napel, and J. S. Ha, "Quantitative 3-D diagnostic ultrasound imaging using a modified transducer array and an automated image tracking technique," *IEEE Trans. Ultrason., Ferroelect., Freq. Contr.*, vol. 49, pp. 1029–1038, Aug. 2002.

[5] X. Wang, C. J. Ritchie, and Y. Kim, "Elevation direction deconvolution in three dimensional ultrasound imaging," *IEEE Trans. Med. Imag.*, vol. 15, pp. 389–394, Jun. 1996.

[6] S. W. Smith, H. G. Pavy, Jr., and O. T. von Ramm, "High-Speed ultrasound volumetric imaging system—Part I: Transducer design and beam steering," *IEEE Trans. Ultrason., Ferroelect., Freq. Contr.*, vol. 38, pp. 100–108, Mar. 1991.

[7] O. T. von Ramm, S. W. Smith, and H. G. Pavy, Jr., "High-Speed ultrasound volumetric imaging system—Part II: Parallel processing and image display," *IEEE Trans. Ultrason., Ferroelect., Freq. Contr.*, vol. 38, pp. 109–115, Mar. 1991.

[8] A. K. Nigam, K. J. Taylor, and G. M. Sessler, "Foil-electret transducer arrays for real-time acoustical holography," in *Acoustical Holography*. vol. 4, G. Wade, Ed. New York: Plenum Press, 1972, pp. 173–197.

[9] N. Takagi, T. Kawashima, T. Ogura, and T. Yamada, "Solid-state acoustic image sensor," in *Acoustical Holography*. vol. 4, G. Wade, Ed. New York: Plenum Press, 1972, pp. 215–236.

[10] J. D. Plummer, R. G. Swartz, M. G. Maginness, J. R. Beaudouin, and J. D. Meindl, "Two-dimensional transmit/receive ceramic piezoelectric arrays: Construction and performance," *IEEE Trans. Sonics Ultrason.*, vol. 25, pp. 273–280, Sep. 1978.

[11] D. H. Turnbull and F. S. Foster, "Fabrication and characterization of transducer elements in two-dimensional arrays for medical ultrasound imaging," *IEEE Trans. Ultrason., Ferroelect., Freq. Contr.*, vol. 39, pp. 464–474, July 1992.

[12] R. L. Goldberg and S. W. Smith, "Multilayer piezoelectric ceramics for two-dimensional array transducer," *IEEE Trans. Ultrason., Ferroelect., Freq. Contr.*, vol. 41, pp. 761–771, Sep. 1994.

[13] J. J. Bernstein, S. L. Finberg, K. Houston, L. C. Niles, H. D. Chen, L. E. Cross, K. K. Li, and K. Udayakumar, "Micromachined high frequency ferroelectric sonar transducers," *IEEE Trans. Ultrason., Ferroelect., Freq. Contr.*, vol. 44, pp. 960–969, Sep. 1997.

[14] M. Greenstein, P. Lum, H. Yoshida, and M. S. Seyed-Bolorforosh, "A 2.5 MHz 2D array with z-axis electrically conductive backing," *IEEE Trans. Ultrason., Ferroelect., Freq. Contr.*, vol. 44, pp. 970–977, Sep. 1997.

[15] J.-M. Bureau, W. Steichen, and G. Lebail, "A two-dimensional transducer array for real-time 3D medical ultrasound imaging," in *Proc. IEEE Ultrason. Symp.*, 1998, pp. 1065–1068.

[16] K. Erikson, A. Hairston, A. Nicoli, J. Stockwell, and T. White, "A $128 \times 128$ ultrasonic transducer hybrid array," in *Proc. IEEE Ultrason. Symp.*, 1997, pp. 1625–1629.

[17] R. E. Davidsen and S. W. Smith, "Two-dimensional arrays for medical ultrasound using multilayer flexible circuit interconnection," *IEEE Trans. Ultrason., Ferroelect., Freq. Contr.*, vol. 45, pp. 338–348, Mar. 1998.

[18] J. O. Fiering, P. Hultman, W. Lee, E. D. Light, and S. W. Smith, "High-density flexible interconnect for two-dimensional ultrasound arrays," *IEEE Trans. Ultrason., Ferroelect., Freq. Contr.*, vol. 47, pp. 764–770, May 2000.

[19] L. Daane and M. Greenstein, "A demountable interconnect system for a 50 x 50 ultrasonic imaging transducer array," *IEEE Trans. Ultrason., Ferroelect., Freq. Contr.*, vol. 44, pp. 978–982, Sep. 1997.

[20] M. Karaman, P.-C. Li, and M. O'Donnell, "Synthetic aperture imaging for small scale systems," *IEEE Trans. Ultrason., Ferroelect., Freq. Contr.*, vol. 42, pp. 429–442, May 1995.

[21] G. R. Lockwood and F. S. Foster, "Optimizing the radiation pattern of sparse periodic two-dimensional arrays," *IEEE Trans. Ultrason., Ferroelect., Freq. Contr.*, vol. 43, pp. 15–19, Jan. 1996.

[22] A. Austeng and S. Holm, "Sparse 2-D arrays for 3-D phased array imaging–design methods," *IEEE Trans. Ultrason., Ferroelect., Freq. Contr.*, vol. 49, pp. 1073–1086, Aug. 2002.

[23] M. Karaman and M. O'Donnell, "Subaperture processing for ultrasonic imaging," *IEEE Trans. Ultrason., Ferroelect., Freq. Contr.*, vol. 45, pp. 429–442, Jan. 1998.

[24] M. Karaman and B. T. Khuri-Yakub, "Low-cost front-end processing for large array systems," in *Proc. 17th Int. Congress Acoust. (ICA'01)*, 2001.

[25] J. A. Johnson, M. Karaman, and B. T. Khuri-Yakub, "Synthetic phased array image formation and restoration," in *Proc. IEEE Int. Conf. Acoust., Speech Signal Processing*, 2002, pp. 2885–2887.

[26] B. T. Khuri-Yakub, C.-H. Cheng, F. L. Degertekin, S. Ergun, S. Hansen, X. C. Jin, and Ö. Oralkan, "Silicon micromachined ultrasonic transducers," *Jpn. J. Appl. Phys.*, vol. 39, pp. 2883–2887, May 2000.

[27] C. H. Cheng, A. S. Ergun, and B. T. Khuri-Yakub, "Electrical through wafer interconnects with 0.05 pico farads parasitic capacitance on 400-$\mu$m thick silicon substrate," in *Proc. Solid-State Sensor, Actuator Microsystems Workshop*, 2002, pp. 157–160.

[28] X. C. Jin, I. Ladabaum, and B. T. Khuri-Yakub, "The microfabrication of capacitive ultrasonic transducers," *IEEE/ASME J. Microelectromech. Syst.*, vol. 7, pp. 295–302, Sep. 1998.

[29] X. C. Jin, I. Ladabaum, F. L. Degertekin, S. Calmes, and B. T. Khuri-Yakub, "Fabrication and characterization of surface micromachined capacitive ultrasonic immersion transducers," *IEEE/ASME J. Microelectromech. Syst.*, vol. 8, pp. 100–114, Mar. 1999.

[30] C.-H. Cheng, E. M. Chow, X. C. Jin, S. Ergun, and B. T. Khuri-Yakub, "An efficient electrical addressing method using through-wafer vias for two-dimensional ultrasonic arrays," in *Proc. IEEE Ultrason. Symp.*, 2000, pp. 1179–1182.

[31] Ö. Oralkan, X. C. Jin, F. L. Degertekin, and B. T. Khuri-Yakub, "Simulation and experimental characterization of a 2-D capacitive micromachined ultrasonic transducer array element," *IEEE Trans. Ultrason., Ferroelect., Freq. Contr.*, vol. 46, pp. 1337–1340, Nov. 1999.

[32] X. C. Jin, Ö. Oralkan, F. L. Degertekin, and B. T. Khuri-Yakub, "Characterization of one-dimensional capacitive micromachined ultrasonic immersion transducer arrays," *IEEE Trans. Ultrason., Ferroelect., Freq. Contr.*, vol. 48, pp. 750–759, May 2001.

[33] Ö. Oralkan, A. S. Ergun, J. A. Johnson, M. Karaman, U. Demirci, K. Kaviani, T. H. Lee, and B. T. Khuri-Yakub, "Capacitive micromachined ultrasonic transducers: Next-generation arrays for acoustic imaging?," *IEEE Trans. Ultrason., Ferroelect., Freq. Contr.*, vol. 49, pp. 1596–1610, Nov. 2002.

[34] S. Calmes, C. H. Cheng, F. L. Degertekin, X. C. Jin, A. S. Ergun, and B. T. Khuri-Yakub, "Highly integrated 2-D capacitive micromachined ultrasonic transducers," in *Proc. IEEE Ultrason. Symp.*, 2000, pp. 1179–1182.

[35] P. C. Eccardt, K. Niederer, T. Scheiter, and C. Hierhold, "Surface micromachined ultrasound transducers in CMOS technology," in *Proc. IEEE Ultrason. Symp.*, 1996, pp. 959–962.

[36] K. Niederer, P.-C. Eccardt, H. Meixner, and R. Lerch, "Micromachined transducer design for minimized generation of surface waves," in *Proc. IEEE Ultrason. Symp.*, 1999, pp. 1137–1139.

[37] R. A. Noble, R. R. Davies, M. M. Day, L. Koker, D. O. King, K. M. Brunson, A. R. D. Jones, J. S. McIntosh, D. A. Hutchins, T. J. Robertson, and P. Saul, "A cost-effective and manufacturable route to the fabrication of high-density 2D micromachined ultrasonic transducer arrays and (CMOS) signal conditioning electronics on the same silicon substrate," in *Proc. IEEE Ultrason. Symp.*, 2001, pp. 941–944.

[38] R. A. Noble, R. R. Davies, D. O. King, M. M. Day, A. R. D. Jones, J. S. McIntosh, D. A. Hutchins, and P. Saul, "Low-temperature micromachined cMUTs with fully-integrated analogue front-end electronics," in *Proc. IEEE Ultrason. Symp.*, 2002, pp. 1045–1050.

[39] M. G. Maginness, J. D. Plummer, W. L. Beaver, and J. D. Meindl, "State-of-the-art in two-dimensional ultrasonic array technology," *Med. Phys.*, vol. 3, pp. 312–318, Oct./Sep. 1976.

[40] U. Demirci, Ö. Oralkan, J. A. Johnson, A. S. Ergun, M. Karaman, and B. T. Khuri-Yakub, "Capacitive micromachined ultrasonic transducer arrays for medical imaging: Experimental results," in *Proc. IEEE Ultrason. Symp.*, 2001, pp. 957–960.

[41] G. G. Yaralioglu, A. S. Ergun, B. Bayram, T. Marentis, and B. T. Khuri-Yakub, "Residual stress and Young's modulus measurement of capacitive micromachined ultrasonic transducer membranes," in *Proc. IEEE Ultrason. Symp.*, 2001, pp. 953–956.

[42] Ö. Oralkan, X. C. Jin, F. L. Degertekin, and B. T. Khuri-Yakub, "Simulation and experimental characterization of a 2-D 3-MHz capacitive micromachined ultrasonic transducer array element," in *Proc. IEEE Ultrason. Symp.*, 1999, pp. 1141–1144.

[43] K. E. Thomenius, "Evolution of ultrasound beamformers," in *Proc. IEEE Ultrason. Symp.*, 1996, pp. 1615–1622.

[44] D. H. Turnbull and F. S. Foster, "Beam steering with pulsed two-dimensional transducer arrays," *IEEE Trans. Ultrason., Ferroelect., Freq. Contr.*, vol. 38, pp. 320–333, July 1991.

[45] J. K. Udupa, "Three-dimensional visualization and analysis methodologies: A current perspective," *Radiographics*, vol. 19, pp. 783–806, May–June 1999.

[46] T. R. Nelson and T. T. Elvins, "Visualization of 3D ultrasound data," *IEEE Comput. Graph. Appl.*, vol. 13, pp. 50–57, Nov. 1993.

**Ömer Oralkan** (S'93) was born in İzmit, Turkey, in 1973. He received the B.S. degree from Bilkent University, Ankara, Turkey, in 1995, and the M.S. degree from Clemson University, Clemson, SC, in 1997, both in electrical engineering. He is currently pursuing a Ph.D. degree in electrical engineering at Stanford University, Stanford, CA.

From 1995 to 1996, he was a hardware and network engineer at Bilkent University Computer Center, Ankara, Turkey. In the summer of 1997, he worked as a process engineer at National Semiconductor Research Laboratories, Santa Clara, CA. His past and present research interests include analog and digital circuit design, micromachined sensors and actuators, and semiconductor device physics and fabrication. His current research focuses on front-end electronic circuit design for 2-D capacitive micromachined ultrasonic transducer arrays for hand-held 3-D ultrasonic imaging systems. He is a corecipient of the Best Paper award presented at the IEEE International Symposium on the Physical and Failure Analysis (IPFA). He is a member of the IEEE.

**A. Sanlı Ergun** (S'96–A'98) was born in Ankara, Turkey, in 1969. He received his B.Sc., M.Sc., and Ph.D. degrees in 1991, 1994, and 1999, respectively, all in electrical and electronics engineering, from Bilkent University, Ankara, Turkey.

He was a research assistant in Bilkent University, Ankara, Turkey, between 1991 and 1999. He is now in the E. L. Ginzton Laboratory, Stanford University as an engineering research associate. His research interests are microwave electronics, ultrasonics, MEMS, and specifically CMUTs. He is a member of the IEEE and the Electron Devices Society.

**Ching-Hsiang Cheng** was born in Taipei, Taiwan. He received the B.S. degree in Mechanical Engineering from National Taiwan University in 1993 and the Master's degrees in both Mechanical and Electrical Engineering from Cornell University in 1998. In the same year, he joined Professor Khuri-Yakub's Ultrasonics Group in Electrical Engineering at Stanford University and is currently pursuing a Ph.D. degree. His research interests include electrical through-wafer interconnects and CMUTs.

**Jeremy A. Johnson** (S'92) received his B.S. in electrical engineering and a minor in mathematics with honors from Walla Walla College, College Place, Washington, in 1997. He received his M.S. in electrical engineering from Stanford University, Stanford, California, in 1999. He is currently pursuing a Ph.D. in electrical engineering from Stanford University.

He has several summers of industry experience. He worked as a software engineer at Interactive Northwest, Inc., during the summer of 1995; worked as an ASIC design engineer at Intel during the summers of 1996 and 1997; performed research in color science at Sony Research Laboratories during the summer of 1998; performed research in computer vision at Hughes Research Laboratories during the summer of 1999; and developed an endoscopic calibration routine for image-enhanced endoscopy at Cbyon, Inc., during the summer of 2000. His research areas include medical imaging, computer-aided diagnosis, and image-guided surgery.

**Mustafa Karaman** (S'88–S'89–M'89–M'93–M'97) received the B.Sc. degree from the Middle East Technical University, Ankara, Turkey, and the M.Sc. and Ph.D. degrees from Bilkent University, Ankara, Turkey, in 1986, 1988, and 1992, respectively, all in electrical and electronics engineering. From 1993 to 1994, he was a postdoctoral fellow in the Biomedical Ultrasonics Laboratory in the Biomedical Department, University of Michigan, Ann Arbor.

From 1995 to 1996, he was on the faculty with the Electrical and Electronics Engineering Department of Kırıkkale University, Turkey, first as Assistant Professor and later as Associate Professor. In 1996, he joined Başkent University, Ankara, Turkey, as the Chairman of Electrical and Electronics Engineering and Acting Chairman of the Computer Engineering Department and served in founding these departments. He was a visiting scholar in the Biomedical Ultrasonics Laboratory at the University of Michigan, Ann Arbor, and in the E. L. Ginzton Laboratory at Stanford University, Stanford, California, in the summer of 1996–1997 and 1999, respectively. Between 2000–2002, he was with the E. L. Ginzton Laboratory at Stanford University, as a visiting/consulting faculty in electrical engineering. In 2002, he joined Işık University, İstanbul, Turkey, where he is currently on the faculty with the Department of Electronics Engineering.

In 1996, Dr. Karaman was awarded H. Tuğaç Foundation Award of Turkish Scientific and Technical Research Council for his contributions to ultrasonic imaging. His research interests include signal/image processing, ultrasonic imaging, and integrated circuit design. Dr. Karaman is a member of the IEEE.

**Thomas H. Lee** (S'87–M'87) received the S.B., S.M., and Sc.D. degrees in electrical engineering from the Massachusetts Institute of Technology, Cambridge, in 1983, 1985, and 1990, respectively.

In 1990, he joined Analog Devices, where he was primarily engaged in the design of high-speed clock recovery devices. In 1992, he joined Rambus Inc., Mountain View, CA, where he developed high-speed analog circuitry for 500-MB/s CMOS DRAMs. He has also contributed to the development of phase-locked loops (PLLs) in the StrongARM, Alpha, and K6/K7/K8 microprocessors. Since 1994, he has been a Professor of electrical engineering at Stanford University, Stanford, CA, where his research focus has been on gigahertz-speed wireline and wireless ICs built in conventional silicon technologies, particularly CMOS.

Dr. Lee cofounded Matrix Semiconductor, authored the textbook *The Design of CMOS Radio-Frequency Integrated Circuits* (Cambridge, U.K.: Cambridge Univ. Press, 1998) and coauthored three books on RF circuit design. He holds 26 U.S. patents.

Dr. Lee is a Distinguished Lecturer of the IEEE Solid-State Circuits Society and the IEEE Microwave Theory and Techniques Society (IEEE MTT-S). He is a two-time recipient of the Best Paper Award presented at the International Solid-State Circuits Conference, a recipient of the Best Paper prize presented at the CICC, and corecipient of a Best Student Paper presented at the International Solid-State Circuits Conference (ISSCC). He holds a Packard Foundation Fellowship.

**Butrus T. Khuri-Yakub** (S'70–S'73–M'76–SM'87–F'95) was born in Beirut, Lebanon. He received the B.S. degree in 1970 from the American University of Beirut, the M.S. degree in 1972 from Dartmouth College, and the Ph.D. degree in 1975 from Stanford University, all in electrical engineering.

He joined the research staff at the E. L. Ginzton Laboratory of Stanford University in 1976 as a Research Associate. He was promoted to a Senior Research Associate in 1978 and to a professor of Electrical Engineering (Research) in 1982. He has served on many university committees in the School of Engineering and the Department of Electrical Engineering. Presently, he is the Deputy Director of the E. L. Ginzton Laboratory. Professor Khuri-Yakub has been teaching both at the graduate and undergraduate levels for over 15 yr, and his current research interests include *in situ* acoustic sensors (temperature, film thickness, resist cure, etc.) for monitoring and control of integrated circuits manufacturing processes, micromachining silicon to make acoustic materials and devices, such as airborne and water immersion ultrasonic transducers and arrays and fluid ejectors, and in the field of ultrasonic nondestructive evaluation and acoustic imaging and microscopy.

Professor Khuri-Yakub is a fellow of the IEEE, a senior member of the Acoustical Society of America, and a member of Tau Beta Pi. He is associate editor of *Research in Nondestructive Evaluation*, a Journal of the American Society for Nondestructive Testing. He has authored over 300 publications and has been principal inventor or coinventor of 52 issued patents. He received the Stanford University School of Engineering Distinguished Advisor Award, June 1987, and the Medal of the City of Bordeaux for contributions to NDE, 1983.